

Characterization of Anatomical Shape Based on Random Walk Hitting Times

Grace Vesom¹, Nathan D. Cahill^{1,2}, Lena Gorelick³, and J. Alison Noble¹

¹ Institute of Biomedical Engineering, University of Oxford, Oxford OX3 HDQ, UK

² Research & Innovation, Carestream Health, Inc., Rochester, NY 14608, USA

³ Computer Vision Group, The Weizmann Institute of Science, Rehovot 76100, Israel

Abstract. This paper presents an implicit shape representation for describing anatomical shapes with high inter-patient variability based on the expected boundary hitting time of a random walk, which happens to be the solution to the Poisson equation. The main contribution of this paper is to test the validity of the Poisson-based mapping for representing anatomical shape, comparing its compactness and completeness with the commonly used Signed Distance Transform and using the liver and the caudate nucleus as examples. Based on these findings, we discuss its use as a shape prior for image segmentation.

1 Introduction

An integral part of modern disease management is treatment planning, which involves several aspects of medical image analysis, from segmenting objects of interest for volume measurement to intra-patient registration to monitor size change or morphology. Because of the difficulty of these tasks, many segmentation or registration frameworks require a shape representation for the object in question. Shape representations can be abstractly divided into two categories: explicit and implicit. Explicit shape representations are parameterized to create ordered collections of components. Examples include Active Shape Models [1] and spherical harmonics [2]. Mostly, they define a $(N - 1)$ -dimensional boundary in a N -dimensional image space, but can include additional information such as a medial representation [3] or, like Active Appearance Models [4], intensity and texture.

An implicit representation of an N -dimensional shape is a function $f(\mathbf{x})$ in an N -dimensional space that takes on the value zero if and only if \mathbf{x} is a position on the $(N - 1)$ -dimensional shape boundary. The mapping is defined over the inside domain of the closed object, and sometimes, depending on the application, over the entire image domain.

Implicit shape descriptions are free of topological constraints and have local support. In recent literature, the Signed Distance Transform (SDT) has proved to be a popular implicit shape representation – attractive for ease of computation, definition over the entire image space, and ability to fit into a level-set segmentation framework. In addition to the SDT, Hong et al. [5] developed an

implicit shape representation based on a Gaussian convolution kernel, which is attractive for its quick computation. Their shape representation is related to the solution of the heat equation, but makes a simplifying assumption that the solution of the heat equation for arbitrary shapes can be found by convolution with a Gaussian kernel.

In our work, we consider another implicit shape representation called the Poisson Transform (PT) and look at its application in modeling anatomical variation. The PT was first used by Gorelick et al. [6] to analyze 2D shape properties on silhouettes in order to perform shape classification and retrieval. We extended that idea in [7] to include the shape exterior and used this in the context of deformable image registration. In the next section, we revisit the mathematical representation of the SDT, then provide a summary of and computational method for the PT. We use this new mapping to produce an implicit shape representation, and then analyze it for completeness and compactness in comparison to the SDT. We use Principal Component Analysis on the SDT for our training shapes to summarize shape variation in the same manner as [8, 9, 10]. We investigate the validity of the SDT shape representation for anatomical shapes with highly variable shape against the PT shape representation. Besides the technical report by Lamecker et al. [11], no studies have assessed the compactness or completeness of the SDT for shape description. We conclude by discussing its application to image segmentation.

2 Implicit Shape Representations

Let us define S to be the interior of the shape and assume that $S \subset \Omega$, where Ω is the entire image space. Then $\partial S = \bar{S} - S$ is the boundary of S , where \bar{S} represents the closure of the open set S .

2.1 Signed Distance Transform

The SDT is also known as the signed Euclidean Distance Transform and is represented mathematically in this paper by W_{SDT} . It yields two pieces of information: the magnitude provides the Euclidean distance between a point and the closest point on ∂S , and the sign indicates whether the current point is inside S (negative) or outside S (positive). Mathematically speaking, W_{SDT} is a solution to the Eikonal equation:

$$\begin{aligned} |\nabla W_{\text{SDT}}(\mathbf{x})| &= 1 \quad \forall \mathbf{x} \in \bar{\Omega}, \\ W_{\text{SDT}}(\mathbf{x}) &= 0 \quad \forall \mathbf{x} \in \partial S. \end{aligned} \tag{1}$$

2.2 Random Walk Hitting Time

Gorelick et al. [6] presented an implicit shape representation based on the expected time for a symmetric random walk to reach the shape boundary. Based

on the solution to Poisson's equation, this representation was shown to have superior behavior than the SDT for shape classification, due to its differentiability and its smoothing of noisy shape boundaries.

Let $U(x, y, z)$ represent the expected random walk hitting time for a particle starting at (x, y, z) inside an open region S to reach any point on the boundary of S , so $U(x, y, z) = 0$ for points on that boundary, i.e., $\forall(x, y, z) \in \partial S$. At every point $(x, y, z) \in S$, $U(x, y, z)$ is equal to the average value of its immediate six neighbors plus a constant (representing the amount of time required to get to an immediate neighbor), i.e.,

$$U(x, y, z) = 1 + \frac{1}{6} \left(U(x+h, y, z) + U(x-h, y, z) \right. \\ \left. U(x, y+h, z) + U(x, y-h, z) \right. \\ \left. U(x, y, z+h) + U(x, y, z-h) \right). \quad (2)$$

Note that (2) is the discrete form of the Poisson equation

$$\Delta U(x, y, z) = -\frac{6}{h^2}, \quad (3)$$

with $\Delta U = U_{xx} + U_{yy} + U_{zz}$ denoting the Laplacian of U , while setting $h = 1$ for our discretized solution.

To use comparable notation with the SDT definition, let W_{PT} replace U to represent the symmetric random walk hitting time to the shape boundary in an open domain, and let $\mathbf{x} = (x, y, z)$ for the remainder of this paper. Also like the SDT, we seek to use the sign of the metric values to define points inside and outside the boundary shape, which results in changing the sign of (3), while the magnitude of those values still provides the symmetric random walk time to a point on the boundary. Thus, for the shape interior, the *Poisson Transform* W_{PT} satisfies

$$\Delta W_{\text{PT}}(\mathbf{x}) = 6 \quad \forall \mathbf{x} \in S, \\ W_{\text{PT}}(\mathbf{x}) = 0 \quad \forall \mathbf{x} \in \partial S. \quad (4)$$

On the exterior of the shape, if no further boundary conditions are prescribed, the random walk analogy fails and the Poisson equation has infinitely many solutions. Therefore, in order to provide an extension of this shape representation to the entirety of $\bar{\Omega}$, we need to define some sort of external boundary condition. One option is to enforce Neumann boundary conditions on $\partial\Omega$; however, this choice gives undesirable behavior of the gradient of the Poisson Transform at the image boundaries. Instead, we choose to define an open sphere $T \supset \bar{\Omega}$ centered on the centroid of Ω , and solve the following boundary value problem:

$$\Delta W_{\text{PT}}(\mathbf{x}) = -6 \quad \forall \mathbf{x} \in T - \bar{S}, \\ \langle \nabla W_{\text{PT}}(\mathbf{x}), \mathbf{n}(\mathbf{x}) \rangle = 0 \quad \forall \mathbf{x} \in \partial T, \\ W_{\text{PT}}(\mathbf{x}) = 0 \quad \forall \mathbf{x} \in \partial S, \quad (5)$$

where $\mathbf{n}(\mathbf{x})$ is the outward pointing normal vector to the surface ∂T at \mathbf{x} . The Neumann boundary condition on ∂T effectively reflects the symmetric random walk in the direction normal to the sphere. Once W_{PT} has been found on T , it can be cropped to $\bar{\Omega}$.

Computing a discrete approximation of W_{PT} inside S can be done in linear time with a multigrid algorithm [6]. This algorithm can be extended to approximate W_{PT} inside $T - \bar{S}$ by appropriately discretizing the Neumann boundary conditions, as established by Cahill et al. [7]. We have found that applying two w-cycles that employ naive boundary conditions at the coarse levels (placing the boundary at the nearest coarse grid points, instead of modifying the nearby coarse equations to account for the fine, pixel-level location of the boundary) provides a good approximation. For further details on the multigrid method, see [12].

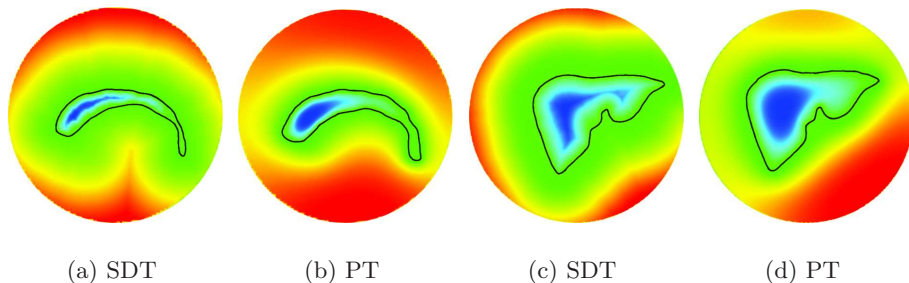


Fig. 1. Slices from example 3D caudate nucleus and liver images of both implicit functions, inside and outside the shape

3 Application to Segmentation

In medical image segmentation, image data information is typically balanced by integrating a priori knowledge into the algorithm through a shape prior, providing a global constraint in a segmentation framework.

3.1 Shape Representation

Using a shape prior for image segmentation requires an application-specific choice of shape representation. Selecting a shape representation is a function of the information to be extracted from an image, the signal-to-noise of the image, the anatomical object in question, and the ultimate goal of the task. For the purpose of segmentation, the shape representation also subsequently affects the dissimilarity measure for comparing shapes and method of integration for

a descriptor or model into a segmentation framework. Golland et al. [13] found that the choice of shape representation changed their classifier function results by about 15%, independent of shape analysis and alignment.

3.2 Shape Analysis Methods

With highly variable anatomical shapes, large numbers of samples, or training shapes, are required to correctly portray a shape population. To efficiently summarize the training shape space, shape analysis is applied to the training shapes resulting in a shape model or descriptor.

Much research looks for the best shape analysis method to summarize the shape space, while some methods never question the validity of its use, such as with Principal Component Analysis (PCA). That method is utilized to reduce the dimensionality of the training shape space, while preserving the most variation. PCA is often challenged because of its sensitivity to low sample size, as well as the assumption of a Gaussian uni-modal distribution for the features measured in the resulting model. In the case of the SDT and PT, the shape representation space is not closed under linear operations, but PCA is still often employed. Shape analysis alternatives include Best Basis Selection [14], principal factor analysis [15], and support vector machines [13]. Additionally, methods to work around obstacles in PCA have shown some success. They transform training data into a feature space via Mercer kernels [16], or transform training data into a vector space using Fourier approximation [17] or the logarithm of odds ratio [18], where linear operations of shape representation transformations are closed.

With the SDT, PCA has been consistently employed for shape analysis for the purpose of creating a statistical shape model. Notwithstanding, Hong et al. [5] used their integral kernel shape representation as a template with a deformation field for segmentation, removing the need for any shape analysis.

3.3 Implicit Anatomical Shape Priors

In image segmentation of highly variable shapes, it is essential to integrate a priori information as a global constraint with data-driven energy functions. We concentrate here on statistical shape models (SSMs), as opposed to deformable shape models or classifiers.

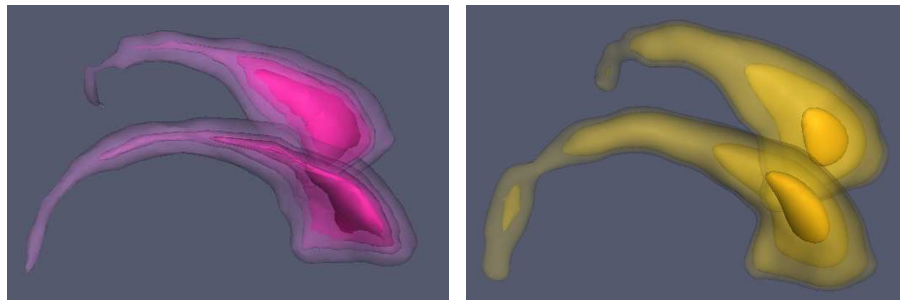
Leventon et al. [8] employed SSMs from implicit shape representations, using the SDT to represent shapes and PCA to summarize the shape space to create a shape prior in image segmentation. Thereafter, literature involving implicit shape models concentrates on shape alignment prior to PCA and shape prior integration into a region-based level-set segmentation framework. Rousson et al. [10] used the sum of squared distances as a dissimilarity measure between the prior and target, while minimizing the rotation and translation pose parameters during the level set evolution. Tsai et al. [9] similarly proposed an alignment method, but also included scale as a pose parameter and explored three energy functionals, approaching the solution through gradient descent. Yang et al. [19]

took another step by introducing neighbor priors, developing a hierarchical multi-object segmentation. Accounting for neighboring structures in the shape prior, however, gave rise to concerns about closedness of linear combination of signed distance functions. Neighboring structures were modeled by the difference of their representative SDTs, however any linear combination of these differences may not represent neighboring structures as mutually exclusive.

3.4 Analysis of Implicit Shape Representations SDT and PT

While PCA may have its drawbacks, it is the most widely used form of shape analysis in medical imaging because of its ease of computation and interpretation. For these reasons, we have thus chosen to use PCA for a comparative shape analysis study on the SDT and PT.

The nature of the PT allows us to combine global and local shape extraction – we can see a common shape for each structure, while local variations are preserved closer to the boundary (Figs. 2(b) and 3(b)). For this reason, we believe PT is best suited to represent objects with high shape variability. Both the liver and caudate nucleus are well known and well studied objects with high shape variability.

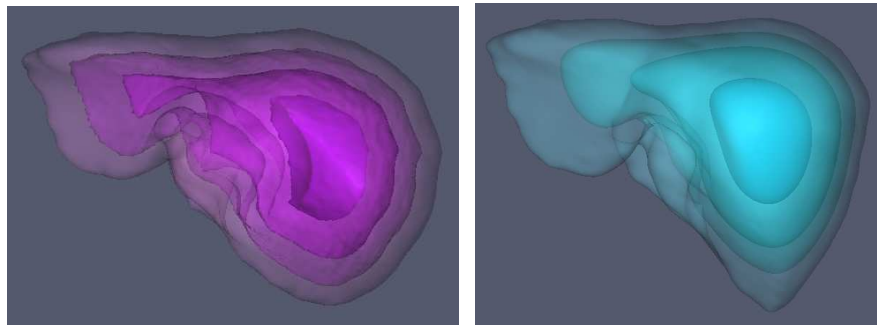


(a) Signed distance function

(b) Poisson function

Fig. 2. Inside level sets of the caudate nucleus from SDT and PT

Consider the case of representing the shape of the liver. Although liver shape has consistent convexities, concavities, and ridges, it is still very highly variable across the population, and is located adjacent to structures of similar density, making it extremely difficult to segment in Computed Tomography (CT) images. Liver image segmentation has been a well-established problem in the medical imaging domain. A variety of published methods range from deformable models using the evolutionary algorithm [20] and data-driven methods [21] to graph-cuts [22], demonstrating the difficulty of the task.



(a) Signed distance function

(b) Poisson function

Fig. 3. Inside level sets of the liver from SDT and PT

As another case study object, the caudate nucleus shape is often investigated in showing brain abnormalities. In disease management for the caudate nucleus, volume measurements are insufficient in indicating change from disease, yet an irregular shape in longitudinal studies and intra-patient asymmetric shape can reveal developmental disorders, such as schizophrenia [23].

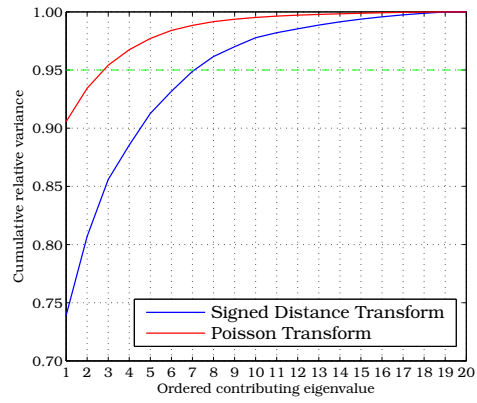
In 3D, we computed the SDT and PT for 33 liver images and 20 caudate nucleus images. Slices through the mapping for each transform and class are shown in Fig. 1, and 3D renderings of the inner level sets are shown in Figs. 2 and 3.

3.5 The Data

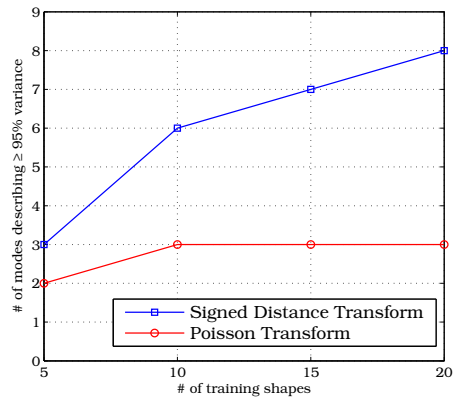
Our data has been obtained from the MICCAI 3D Segmentation Challenge [24] and the Churchill Hospital, part of the Oxford Radcliffe Hospitals NHS Trust in Oxford, UK. We used the segmented training data sets from MICCAI, and manually segmented the additional liver data sets, which were approved by a clinician. All binary images were rescaled to physical Cartesian coordinates, and smoothed to remove aliasing effects. The liver surfaces were aligned as binary images using the Principal Axis Transformation [25], while the caudate nucleus shapes were aligned using first-order moments, with a few slight manual rotations.

3.6 Analysis

For each case, we ran PCA over the entire data set, Figs. 4(a) and 5(a), and then for randomly chosen sets in multiples of 5, to show the number of modes needed to summarize a cumulative variance threshold of 95% given the changing number of training shapes, Figs. 4(b) and 5(b).

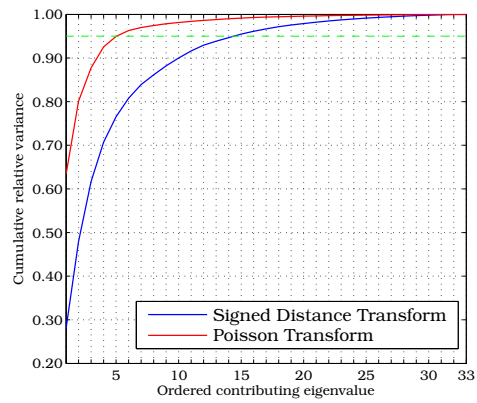


(a) Cumulative relative variance for entire dataset

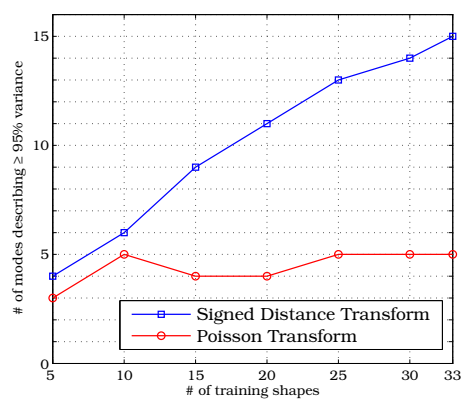


(b) Modes needed to cover 95% of variance with varying number of training shapes

Fig. 4. Compactness and completeness of the SDT and PT for the shape of the caudate nucleus



(a) Cumulative relative variance for entire dataset



(b) Modes needed to cover 95% of variance with varying number of training shapes

Fig. 5. Compactness and completeness of the SDT and PT for the shape of the liver

We defined compactness of a shape description as requiring as few parameters as possible and show relative compactness here in comparison to the SDT. From Figs. 4(a) and 5(a), we see that to summarize 95% of shape variance for the caudate nucleus and the liver, the SDT requires 8 and 15 modes, while the PT requires only 3 and 5, respectively – approximately a 3-fold improvement in both cases.

3.7 Discussion

PCA is argued to be incomplete, that is to say some actual shapes may be unrealizable from the basis, which is chosen for low-approximation while summarizing the most variance. However, one can argue that that is dependent on what has been extracted into the shape representation. Boundary representations give information about the object delineation, and SDT-maps propagate boundary variations throughout the domain where the function is defined. However, the PT-maps reveal common and underlying shapes inwards, as the boundary variations smooth quickly away from the surface (see Figs. 1–3).

With a large number of training data, the number of modes required should level off, as we would expect in a complete shape descriptor. If the number of modes required grows with the number of training data, then it can be inferred that every randomly chosen set of 5 training data added were somehow orthogonal to the existing set, which is improbable. Then PCA might be incapable of accurately reducing the dimensionality of a shape space spanned by the SDT on liver and caudate nucleus shapes.

For a SSM based on the liver for image segmentation, Lamecker et al. [11] used a subsampled geometric mesh representation. Mesh point values, like all values in a SDT-map, are directly affected by any noise on the shape surface. Lamecker report compactness and completeness curves consistent with that of the signed distance function in their liver SSM analysis, and required 18 modes to summarize 95% variance for 33 training shapes and 21 modes for 42 training shapes.

In contrast, the PT completeness curve flattens quickly as the number of training shapes grows, converging to a fixed number of modes, as we should expect in a complete model (Fig. 5(b)). Through our analysis we can see the PT is a relatively more compact and complete shape representation than SDT.

4 Conclusion and Future Work

In this paper, we introduced using a new implicit shape representation called the Poisson Transform, an extrapolation of Gorelick’s innovative approach to shape characterization. We argued its validity over the SDT in a PCA shape analysis. We are currently working on methods of integrating a shape descriptor based on the PT into an image segmentation framework and overcoming obstacles mentioned in [13, 18].

Acknowledgments

The authors would like to thank Professor J. M. Brady for his discussions; Tobias Heimann, Martin Styner, and Bram van Ginneken for allowing us to use their data; and Dr. Joanne Brady from the Churchill Hospital in Oxford for selecting patients and overseeing manual segmentations.

References

- [1] T. Cootes, C. Taylor, D. Cooper, J. Graham, *et al.*, “Active shape models—their training and application,” *Computer Vision and Image Understanding*, vol. 61, no. 1, pp. 38–59, 1995.
- [2] C. Brechbuhler, G. Gerig, and O. Kubler, “Parametrization of closed surfaces for 3-D shape description,” *Computer Vision and Image Understanding*, vol. 61, no. 2, pp. 154–170, 1995.
- [3] M. Styner and G. Gerig, “Medial models incorporating object variability for 3D shape analysis,” *Information Processing in Medical Imaging*, pp. 502–516, 2001.
- [4] T. Cootes, G. Edwards, and C. Taylor, “Active appearance models,” *IEEE Transactions on Pattern Analysis and Machine Intelligence*, vol. 23, no. 6, pp. 681–685, 2001.
- [5] B.-W. Hong, E. Prados, S. Soatto, and L. Vese, “Shape Representation based on Integral Kernels: Application to Image Matching and Segmentation,” in *Proc. CVPR*, pp. I: 833–840, 2006.
- [6] L. Gorelick, M. Galun, E. Sharon, R. Basri, and A. Brandt, “Shape Representation and Classification Using the Poisson Equation,” *Transactions on Pattern Analysis and Machine Intelligence*, vol. 28, no. 12, pp. 1991–2005, 2006.
- [7] N. D. Cahill, G. Vesom, L. Gorelick, J. Brady, J. A. Noble, and J. M. Brady, “Investigating Implicit Shape Representations for Alignment of Livers from Serial CT Examinations,” in *Proc. International Symposium on Biomedical Imaging*, May 2008.
- [8] M. E. Leventon, W. E. L. Grimson, and O. Faugeras, “Statistical shape influence in geodesic active contours,” in *Computer Vision and Pattern Recognition, 2000. Proceedings. IEEE Conference on*, vol. 1, pp. 316–323, 2000.
- [9] A. Tsai, A. Yezzi Jr, W. Wells, C. Tempany, D. Tucker, A. Fan, W. Grimson, and A. Willsky, “A shape-based approach to the segmentation of medical imagery using level sets,” *Medical Imaging, IEEE Transactions on*, vol. 22, no. 2, pp. 137–154, 2003.
- [10] M. Rousson, N. Paragios, and R. Deriche, “Implicit Active Shape Models for 3D Segmentation in MR Imaging,” in *MICCAI 2004*, vol. 3216, pp. 209–216, Springer Berlin / Heidelberg, September 2004.
- [11] H. Lamecker, T. Lange, and M. Seebass, “Segmentation of the Liver using a 3D Statistical Shape Model,” tech. rep., Zuse Institute Berlin, April 2004.
- [12] U. Trottenberg, C. W. Oosterlee, and Schüller, *Multigrid*. Academic Press, 2001.
- [13] P. Golland, W. Grimson, M. Shenton, and R. Kikinis, “Detection and analysis of statistical differences in anatomical shape,” *Medical Image Analysis*, vol. 9, pp. 69–86, February 2005.
- [14] A. Mohamed and C. Davatzikos, “Shape Representation via Best Orthogonal Basis Selection,” in *Medical Image Computing and Computer-Assisted Intervention MICCAI 2004*, pp. 225–233, 2004.

- [15] M. Ballester, M. Linguraru, M. Aguirre, and N. Ayache, "On the adequacy of principal factor analysis for the study of shape variability," *Proc. SPIE*, vol. 5747, pp. 1392–1399, 2005.
- [16] D. Cremers, T. Kohlberger, and C. Schnörr, "Shape statistics in kernel space for variational image segmentation," *Pattern Recognition*, vol. 36, pp. 1929–1943, September 2003.
- [17] A. Srivastava, S. H. Joshi, W. Mio, and X. Liu, "Statistical shape analysis: clustering, learning, and testing," *Pattern Analysis and Machine Intelligence, IEEE Transactions on*, vol. 27, no. 4, pp. 590–602, 2005.
- [18] K. M. Pohl, J. Fisher, M. Shenton, R. McCarley, W. Grimson, R. Kikinis, and W. Wells, "Using the logarithm of odds to define a vector space on probabilistic atlases," *Medical Image Analysis*, vol. 11, pp. 465–477, October 2007.
- [19] J. Yang, L. H. Staib, and J. S. Duncan, "Neighbor-constrained segmentation with level set based 3-D deformable models," *Medical Imaging, IEEE Transactions on*, vol. 23, no. 8, pp. 940–948, 2004.
- [20] T. Heimann, S. Munzing, H. Meinzer, and I. Wolf, "A Shape-Guided Deformable Model with Evolutionary Algorithm Initialization for 3D Soft Tissue Segmentation," in *Information Processing in Medical Imaging*, vol. 4584, pp. 1–12, Springer Berlin/Heidelberg, 2007.
- [21] L. Soler, H. Delingette, G. Malandain, J. Montagnat, N. Ayache, C. Koehl, O. Dourthe, B. Malassagne, M. Smith, D. Mutter, *et al.*, "Fully automatic anatomical, pathological, and functional segmentation from CT scans for hepatic surgery," *Computer Aided Surgery*, vol. 6, no. 3, pp. 131–142, 2001.
- [22] Y. Boykov and G. Funka-Lea, "Graph Cuts and Efficient N-D Image Segmentation," *International Journal of Computer Vision*, vol. 70, pp. 109–131, November 2006.
- [23] J. Levitt, C. Westin, P. Nestor, R. Estepar, C. Dickey, M. Voglmaier, L. Seidman, R. Kikinis, F. Jolesz, R. McCarley, *et al.*, "Shape of caudate nucleus and its cognitive correlates in neuroleptic-naive schizotypal personality disorder," *Biological Psychiatry*, vol. 55, no. 2, pp. 177–184, 2004.
- [24] B. van Ginneken, T. Heimann, and M. Styner, "3D Segmentation in the Clinic: A Grand Challenge," in *3D Segmentation in the Clinic: A Grand Challenge* (B. van Ginneken, T. Heimann, and M. Styner, eds.), pp. 7–15, 2007.
- [25] N. M. Alpert, "The Principal Axes Transformation—A Method for Image Registration," *Journal of Nuclear Medicine*, vol. 31, pp. 1717–1722, October 1990.